THE JOURNAL OF BIOLOGICAL CHEMISTRY Vol. 278, No. 42, Issue of October 17, pp. 41093–41098, 2003

Printed in U.S.A.

Crystal Structure of *Pasteurella haemolytica* Ferric Ion-binding Protein A Reveals a Novel Class of Bacterial Iron-binding Proteins*

Received for publication, June 26, 2003, and in revised form, July 25, 2003
Published, JBC Papers in Press, July 25, 2003, DOI 10.1074/jbc.M306821200

Stephen R. Shouldice‡§, Douglas R. Dougan§¶, Pamela A. Williams‖, Robert J. Skene¶, Gyorgy Snell¶, Daniel Scheibe¶, Shane Kirby‡, David J. Hosfield¶, Duncan E. McRee¶, Anthony B. Schryvers‡, and Leslie W. Tari¶**

From the ‡Department of Microbiology and Infectious Diseases, University of Calgary, Calgary, Alberta T2N 4N1, Canada, ¶Syrrx, Inc., San Diego, California, 92121, and ‖Astex Technology, Cambridge CB4 0QA, United Kingdom

Pasteurellosis caused by the Gram-negative pathogen *Pasteurella haemolytica* is a serious disease leading to death in cattle. To scavenge growth-limiting iron from the host, the pathogen utilizes the periplasmic ferric ion-binding protein A (PhFbpA) as a component of an ATP-binding cassette transport pathway. We report the 1.2-Å structure of the iron-free (apo) form of PhFbpA, which is a member of the transferrin structural superfamily. The protein structure adopts a closed conformation, allowing us to reliably assign putative iron-coordinating residues. Based on our analysis, PhFbpA utilizes a unique constellation of binding site residues and anions to octahedrally coordinate an iron atom. A surprising finding in the structure is the presence of two formate anions on opposite sides of the iron-binding pocket. The formate ions tether the N- and C-terminal domains of the protein and stabilize the closed structure, also providing clues as to probable candidates for synergistic anions in the iron-loaded state. PhFbpA represents a new class of bacterial iron-binding proteins.

Pasteurella haemolytica is the causative agent of the bovine respiratory disease called shipping fever or pneumonic pasteurellosis (1). Bovine pneumonic pasteurellosis is the final stage of a complex multifactorial process typically involving stress and infectious organisms leading to pneumonia in cattle. Respiratory disease is a major cause of morbidity in the cattle industry resulting in a significant economic loss. In healthy cattle, *P. haemolytica* is present in low numbers in the nasal passages. However, following stress conditions such as shipment, commingling cattle from different sources, and overcrowding, respiratory disease may result in which the opportunistic pathogen *P. haemolytica* is the predominant bacteria isolated and responsible for acute lung injury (1, 2). While under stress, proliferation of *P. haemolytica* is facilitated, leading to infection of the upper respiratory tract and eventual colonization of the lower airway (3). In the past, vaccine trials aimed at preventing disease due to *P. haemolytica* have met with difficulties and limited success (4, 5). Investigators have noted that for many Gram-negative pathogenic bacteria, iron acquisition directly corresponds to virulence (6, 7). Iron is an integral nutrient for the survival of nearly all organisms and is an essential cofactor of numerous metabolic and enzymatic processes (7, 8). Therefore, researchers believe that proteins expressed under iron-limited conditions may be essential for bacterial survival and may ultimately serve as therapeutic targets.

Iron is abundant in the environment and should not be a limiting factor for growth. However, under aerobic conditions and at neutral or alkaline pH, aqueous iron precipitates as an insoluble Fe^{3+} hydroxide. Furthermore, free iron can generate toxic derivatives within the body (9). Thus, it is vital that biological systems maintain control of the chemical environment of iron. The mammalian host utilizes the monomeric, bilobal, and iron-binding glycoproteins transferrin (Tf)[1] (in sera) and lactoferrin (on mucosal surfaces) to limit the amount of free iron available to pathogens and transport iron throughout the body.

In response to the problem of iron scarcity, the extracellular Gram-negative pathogens of the *Pasteurellaceae* and *Neisseriaceae* families have developed high affinity iron acquisition systems to obtain this essential nutrient (10). Three components are involved in the successful uptake of iron from the eukaryotic host Tf as follows: (i) an outer membrane Tf receptor complex; (ii) an inner membrane-associated TonB complex; and (iii) an ATP-binding cassette (ABC)-type ferric ion transporter system. The host-specific bacterial outer membrane Tf receptor is composed of two proteins, Tf-binding proteins A (TbpA) and B (TbpB) (11). The TbpB receptor component is largely an extracellular hydrophilic macromolecule, which is anchored to the outer membrane through a lipidated tail (11). TbpA is a TonB-dependent integral membrane protein that is proposed to mediate transport of iron across the outer membrane. The transport of iron across the outer membrane requires the presence of a functional TonB protein (12). Following the removal of iron from transferrin and translocation across the outer membrane, the ferric ion is complexed by a periplasmic ferric ion-binding protein (FbpA). Studies have revealed the function of FbpA in complexing and transporting iron across the periplas

* This work was supported by Grant 49603 from the Canadian Institutes for Health Research. This work is based on diffraction experiments conducted at the ALS. The costs of publication of this article were defrayed in part by the payment of page charges. This article must therefore be hereby marked "*advertisement*" in accordance with 18 U.S.C. Section 1734 solely to indicate this fact.

The atomic coordinates and structure factors (code 1Q35) have been deposited in the Protein Data Bank, Research Collaboratory for Structural Bioinformatics, Rutgers University, New Brunswick, NJ (http://www.rcsb.org/).

§ Both authors contributed equally to this work.

** To whom correspondence should be addressed: Associate Director, Crystallography, Syrrx Inc., 10410 Science Center Dr., San Diego, CA, 92121. Tel.: 858-622-8528 (ext. 3624); Fax: 858-550-0598; E-mail: ltari@syrrx.com.

[1] The abbreviations used are: Tf, transferrin; ABC, ATP-binding cassette; TbpA, Tf-binding protein A; TbpB, transferrin-binding protein B; Fbp, ferric ion-binding protein; PhFbpA, *P. haemolytica* ferric ion-binding protein; PEG, polyethylene glycol; HiFbpA, *H. influenzae* periplasmic FbpA; PDB, Protein Data Bank; PLBP, periplasmic ligand-binding protein.

mic space (13–15) as the periplasmic component of the iron ABC transport system (16). The ABC family of transporters includes a broad and diverse group of import systems found in prokaryotes. ABC transporters generally consist of separate polypeptides that form an $A_1B_2C_2$ complex at the inner membrane of the cell during transport. Thus, in order for the ferric ion to reach the cytoplasm, it is donated to an inner membrane complex consisting of the inner transmembrane protein FbpB and the cytoplasmic ATPase FbpC. This high affinity bacterial iron uptake system results in iron from host transferrin being liberated at the cell surface, translocated through the periplasmic space, and deposited into the cytoplasm for use or storage without the incorporation of the transferrin protein into the bacterial cell.

Because the FbpABC pathway appears to be a common route for ferric iron uptake from several different sources, it is a particularly attractive therapeutic target. Identification of the gene encoding PhFbpA was based on complementation of an *entA Escherichia coli* strain transformed with a *P. haemolytica* λZAP II library-derived plasmid (15). Nucleotide sequence analysis of the *fbpA* gene confirmed homology with the cluster I group of the periplasmic binding protein family (15, 16). Despite its homology to FbpA molecules of other organisms, PhFbpA has a peak-visible absorbance at 419 nm, which is significantly blue-shifted relative to the peak absorbance for other FbpAs (13, 17). PhFbpA shares approximately the same iron affinity as transferrin and other FbpA molecules based on citrate competition assays (15). Thus, current evidence indicates that PhFbpA binds and transports Fe^{3+} ion, utilizing a unique iron-coordinating environment when compared with transferrin or any other biochemically characterized FbpA molecules.

In this study, we describe the 1.2-Å resolution structure of PhFbpA. This is the first example of a closed apoFbpA molecule. Although the structure does not contain a metal atom, the putative metal coordinating residues are clearly evident. The current structure explains how this protein may coordinate iron and the possible locations and identities of synergistic anions.

EXPERIMENTAL PROCEDURES

Purification and Crystallization Procedures—E. coli BL21(DE3)/pLysS harboring the pT7–7 plasmid encoding FbpA was utilized to express the native *P. haemolytica* 35-kDa ferric ion-binding protein A in the periplasm under isopropyl-1-thio-β-D-galactopyranoside induction. A selenomethionine version was also produced using the same plasmid in an *E. coli* strain that is a methionine auxotroph. This strain was grown overnight at 37 °C on M9 minimal media supplemented with ampicillin to 100 μg/ml and methionine to 40 μg/ml. The following day, the culture was inoculated to LeMaster's media. The medium was supplemented with ampicillin (100 μg/ml), selenomethionine (40 μg/ml), and Isovitalex to a 1% v/v final concentration. The culture was grown overnight with shaking at 37 °C and the following day inoculated to fresh media to an A_{600} of 0.05 and induced with isopropyl-1-thio-β-D-galactopyranoside once the culture reached an A_{600} of 0.5. The culture was grown overnight with shaking at 37 °C, and cells were harvested the following day. Both versions of protein were then purified using a modified osmotic shock procedure (18). The supernatant was carefully removed without disrupting the pellet because the supernatant contains the periplasmic osmotic shock fraction. Finally, the sample was extensively dialyzed against 20 mM ethanolamine buffer, pH 9.0, at 4 °C.

Following dialysis, the protein sample was subjected to anion-exchange chromatography on the Akta fast protein liquid chromatography system as a final purification step. The column was washed with 20 volumes of 20 mM ethanolamine buffer, pH 9.0, to remove unbound proteins and eluted with a gradient of 0–1.6 M NaCl. The material collected from the column was concentrated to a final volume of between 1 and 3 ml using a Centricon 10 microconcentrator. At this point, the protein still in the Centricon was exhaustively exchanged into 10 mM Tris-HCl buffer, pH 8.0. Once completed, the samples were concentrated to a final concentration of ~25 mg/ml. The resulting preparations were deemed pure based on SDS-PAGE analysis (data not shown). Protein samples were stored at −80 °C until they were used for crystallography.

The sitting-drop vapor-diffusion method was employed for crystallization of the proteins. The selenomethionyl-PhFbpA crystallization experiments used 2 μl of sitting drops containing 1 μl selenomethionyl-FbpA and 1 μl of reservoir mixture equilibrated against a 1-ml reservoir. Crystals of the protein grew at 20 °C in 96 h from a drop-containing protein (8.5% PEG 5000 and 0.1 M sodium-HEPES, pH 7.0) that was equilibrated against a reservoir containing 17% PEG 5000 and 0.2 M sodium-HEPES, pH 7.0. Diffraction quality crystals belonged to the orthorhombic space group $P2_12_12$ (a = 69.4 Å; b = 106.2 Å; c = 89.84 Å).

Crystals of native PhFbpA were grown at 4 °C from nanovolume drops using the proprietary high throughput protein crystallization platform developed at Syrrx Inc. Each vapor-diffusion experiment used 100-nl sitting drops containing 50 nl of PhFbpA and 50 nl of reservoir mixture equilibrated against a 100-μl reservoir. Colorless crystals of the native protein grew in 72 h from a drop-containing protein (10% PEG 3350 and 0.1 M magnesium formate, pH 5.9) that was equilibrated against a reservoir containing 20% PEG 3350 and 0.2 M magnesium formate, pH 5.9. These crystals were suitable for x-ray diffraction and belonged to the orthorhombic space group $C222_1$ (a = 97.2 Å; b = 189.3 Å; c = 45.8 Å).

Crystal Harvesting and Data Collection—The crystals were harvested by scooping them with a nylon loop. The native crystal was then dipped into a cryoprotectant solution containing 30% (v/v) ethylene glycol, 20% (w/v) PEG 3350, and 0.2 M magnesium formate, pH 5.9, for ~30 s before they were cooled in liquid nitrogen, whereas the selenomethionine crystal was frozen by dipping the crystals in the crystallization mother liquor supplemented with 35% PEG 400. Crystals were kept at 100 K during data collection by use of a nitrogen gas stream. Native diffraction data were collected from a crystal of the PhFbpA sample using an ADSC Quantum 4 detector at beamline 5.0.3 at the Advanced Light Source (ALS, Berkeley, CA) using a wavelength of 1.0 Å. The three-wavelength selenium-multiwavelength anomalous dispersion data sets were collected at the Stanford Synchrotron Radiation Laboratory on beamline 9-2. The data for all of the experiments were reduced and scaled using the HKL2000 software (19). The statistics for all of the data sets are given in Table I.

Structure Determination—Crystals of the selenomethionyl protein were of highly variable quality and diffracted to poor resolution (2.8–3.5-Å resolution). In addition, the subsequent structure determination revealed that the lattice was comprised of two molecules in the asymmetric unit, one ordered molecule and one that was dynamically disordered. However, the selenomethionyl protein crystals were of sufficient quality to obtain an initial trace of the protein that was used to solve the native structure. The selenium sites were located using the program SnB (20). Refinement of the heavy atom sites and phasing calculations were carried out using the program SHARP (21). The resulting electron density maps were interpreted using the program XtalView/Xfit (22), and the model was refined against a maximum likelihood target using the program CNS (23). The high resolution native crystal structure was determined by a molecular replacement procedure using the program Molrep from the CCP4 suite of programs (24). The coordinates of the wild type selenomethionine-PhFbpA were used as the search model. Because the structure of selenomethionine-PhFbpA was in an open conformation compared with the title complex, two independent search models comprising the N- and C-terminal domains of the protein had to be positioned independently to solve the structure. Iterative cycles of interactive manual refitting of the model using the program XtalView/Xfit (22) made use of maps created with ARP/wARP 5.2 (25), and refinement with Refmac5 (26) was carried out to complete and correct the model. Restrained refinement using a maximum likelihood target function and anisotropic temperature factors for individual atoms was carried out. During the later stages of refinement, difference maps ($F_o - F_c$ maps) were used to place the bound ethylene glycol, formate, and water molecules. The final crystallographic R-factor is 0.171 for all of the data from 35.3–1.2-Å resolution. The free R calculated using 5% of the data is 0.195.

Structure Analysis—The refined coordinates of *P. haemolytica* FbpA have been deposited in the Protein Data Bank. Ramachandran plots show the satisfactory location of all of the residues into allowed regions of conformational space. The DALI server (www2.ebi.ac.uk/dali) was utilized in to find structurally similar proteins in the Fold classification based on Structure-Structure alignment of Proteins (FSSP) data base (27).

TABLE I
Summary of crystallographic data

Protein	Native	Se-Met inflection point	Se-Met peak	Se-Met high energy remote
Data collection				
Wavelength (Å)	1.00	0.9796	0.9794	0.9252
Resolution (Å)	95–1.2	40–2.8	40–2.8	40–2.8
Space Group	$C222_1$	$P2_12_12$	$P2_12_12$	$P2_12_12$
Unit cell dimensions (Å)	$a = 97.16$, $b = 189.33$, $c = 45.76$	$a = 69.40$, $b = 106.20$, $c = 89.84$	$a = 69.4$, $b = 106.2$, $c = 89.84$	$a = 69.4$, $b = 106.2$, $c = 89.84$
Completeness (%)[a]	93.4 (65.7)	94.8 (86.5)	95.9 (88.3)	97.6 (90.1)
$I/\sigma(I)$	24.7 (2.6)	10.7 (2.0)	11.4 (2.4)	10.9 (2.1)
R_{sym}[b]	0.036 (0.256)	0.087 (0.435)	0.083 (0.392)	0.085 (0.411)
Overall Figure of Merit (MAD phasing)	NA			0.64
Refinement statistics				
Resolution (Å)	35.3–1.2			8.0–2.8
Completeness (%)	93.3			97.5
No. of reflections	116923			18182
Working set	110753			16363
Free set	6170			1817
R-factor[c]	0.171			0.39
R_{free}	0.195			0.43
No. of Protein atoms	5060			4896
No. of Waters	612			0
Mean B-factors (Å^2)	12.01			41.44
R.m.s.d.				
Bond lengths (Å)	0.006			0.080
Bond angles (°)	1.094			5.028

[a] Numbers in parentheses are the statistics for the highest resolution shell.
[b] $R_{sym} = \Sigma_h (\Sigma_j |I_{j,h} - \langle I_h \rangle| / \Sigma I_{j,h})$, where h = set of Miller indices and j = set of observations of reflection h.
[c] *R*-factor = $\Sigma_{hkl} |F_o - F_c| / \Sigma_{hkl} |F_o|$.

RESULTS

Crystallization and Structure Solution—The recombinant PhFbpA mutant protein was isolated from the periplasm of *E. coli* and purified by ion-exchange chromatography. Following purification, protein samples were concentrated to 25 mg/ml prior to crystallization. Crystals of a selenomethionyl-PhFbpA derivative were used to obtain an initial model. However, the crystals of the selenomethionyl protein diffracted poorly because of the fact that one of the molecules of the two in the asymmetric unit was highly disordered. This necessitated the search for a new crystal form. A superior crystal form was found for the native protein using the Syrrx high throughput nanovolume sitting-drop method, which allowed us to do an extensive search of chemical space. Numerous attempts to grow iron-loaded crystals of PhFbpA have as yet failed to yield a usable crystal form for data collection. The PhFbpA structure presented here was solved by molecular replacement using the selenomethionyl-PhFbpA structure as a model (see "Experimental Procedures").

Structural Features—Phasing and refinement statistics are reported in Table I. For almost all of the protein residues, the electron density is clear and unambiguous. The last two residues of the C terminus and residue 37 were not visible in the electron density map and were omitted. Electron density for side chains of surface exposed residues 208 and 318 was also missing and were built as alanine and glycine, respectively. The crystal structure of PhFbpA is of high quality as evidenced by the stereochemical parameters (Table I) and the Ramachandran plot, which reveals that all of the residues are in allowed regions (as defined in the program PROCHECK) (24).

Crystal structures of all of the FbpA molecules deposited to date demonstrate an almost identical topology. PhFbpA has a similar overall structure to the holo-form of wild type *Haemophilus influenzae* periplasmic FbpA (HiFbpA) with approximate dimensions of 60 × 30 × 40 Å. A search using the DALI (27) server for proteins with similar three-dimensional folds to PhFbpA in the PDB reveals that PhFbpA possesses the highest structural similarity with HiFbpA (PDB code 1MRP, see Ref. 28) (PhFbpA and HiFbpA share 23% sequence identity) and a lesser but significant degree of similarity to most other periplasmic ligand-binding proteins as well as the N-terminal lobes of transferrin (29), lactoferrin (30), and ovotransferrin (31). 301 of 309 Cα atoms of PhFbpA and HiFbpA can be overlaid with a root mean square deviation of 2.3 Å. Similar to other FbpA structures, the polypeptide chain crosses between the N- and C-terminal domains twice. PhFbpA, similar to HiFbpA and most other periplasmic binding proteins as well as transferrins, is composed of two structural domains termed the N- and C-domains. A deep ligand-binding cleft is located at the interface between the two domains. Each domain is composed of a twisted mixed β-sheet surrounded by α-helices (Fig. 1). The two domains are connected by two anti-parallel β-strands, which form the hinge between the two domains. Rotation of the N- and C-terminal domains around this hinge region involving the two β-strands at the base of the ligand-binding cleft (residues 95–109 and 225–238) converts the protein from an open to closed conformation. The PhFbpA structure observed in the selenomethionyl-PhFbpA crystal form (data not shown) adopts an open conformation, which differs from the native PhFbpA structure by a rigid body rotation of the N- and C-lobes around the β-strand hinge by ~20°.

Iron and Anion-binding Sites—Based on our structural analysis and sequence comparisons of PhFbpA with orthologs (Table II and see "Discussion"), we propose that PhFbpA coordinates a single Fe^{3+} ion in an octahedral fashion, utilizing four protein side chains to form the square-planar base of the octahedron with two anions disposed on either side of the base completing the coordination sphere (Figs. 2 and 3). The four residues comprising the base of the octahedron are Gln-11, Tyr-142, Tyr-198, and Tyr-199. With the exception of Gln-11, all of the putative iron-binding residues (and anions) lie within hydrogen-bonding distance of one another and through small rearrangements could satisfy the requirements for octahedral iron coordination. Although the Tyr residues located deep in the binding cleft are well described by electron density, the terminus of the Gln-11 side chain, which resides on a surface loop emanating from the pocket rim, is poorly ordered. The amide of Gln-11 points away from the binding pocket and is

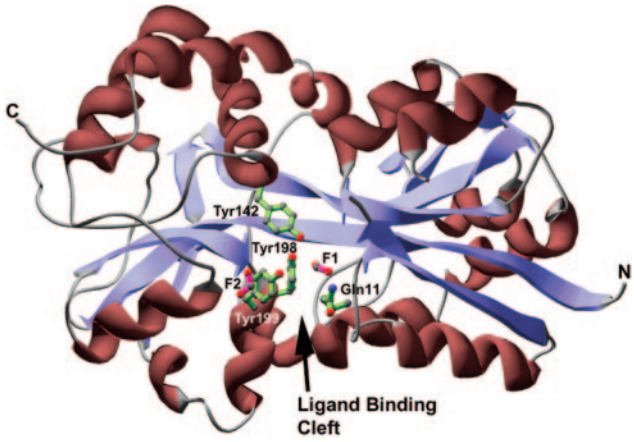

FIG. 1. **Ribbon diagram of PhFbpA structure.** PhfbpA possesses two α/β-domains linked by a β-strand hinge. α-Helices are shown in *purple*, whereas β-strands are shown in *blue*. The relative positions of the two formate anions (*F1* and *F2*) and putative iron ligands in the binding cleft are shown. For reference, the orientation of the protein shown here is the orientation used to generate Fig. 3.

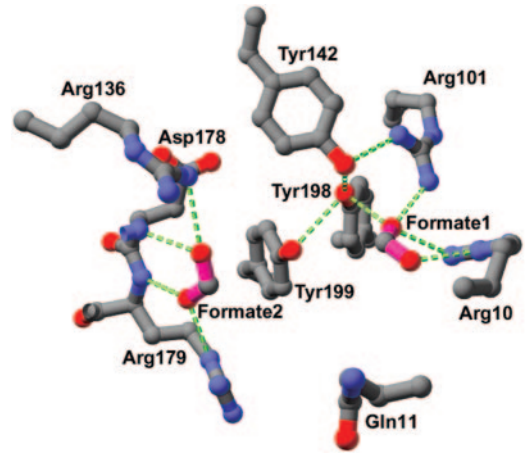

FIG. 2. **Detailed view of the PhFbpA-binding pocket.** Potential hydrogen-bonding interactions are shown as *green dotted lines*. Through small positional rearrangements, Gln-11, Tyr-142, Tyr-198, and Tyr-199 could form a square planar base around a bound ferric ion, whereas carbonate ions could bind in the formate ion positions and complete the octahedral coordination sphere.

TABLE II
Amino acid sequence comparisons

Sequence comparison comparing key putative iron and anion binding residues in PhFbpA to ortholog proteins. Homologous sequences were found and aligned using BLAST (32). Residues conserved between PhFbpA and ortholog proteins are designated by an X, and groups with non-conserved amino acids are shown. The groups are designated as follows: Group 1 (amino acid identity 50–80%, BLAST score 324–511) *Pasteurella multocida*, *Haemophilus somnus*, *Vibrio parahaemolyticus*, *Vibrio cholerae*, *Shewanella oneidensis*, *Rhodospirillum rubrum*, *Rhodobacter sphaeroides*, *Sinorhizobium melioloti*, and *Agrobacterium tumefaciens*; group 2 (amino acid identity 46–52%, BLAST score 286–331) *Rhodopseudomonas palustris*, *Brucella melitensis*, *Brucella suis*. *A. tumefaciens*; group 3 (amino acid identity 37–41%, BLAST score 201–231) Synechocystis sp., *Burkholderia fungorum*, *Trichodesmium erythraeum*, *Thermosynechococcus elongates*, *Synechococcus* sp., *Campylobacter jejuni*, and *Clostridium perfringens*; group 4 (amino acid identity 41%, BLAST score 228) *Ehrlichia chaffeensis*.

	Group 1	Group 2	Group 3	Group 4
Arg^{10}	X	X	X	X
Gln^{11}	X	Glu	His	Lys
Arg^{101}	X	X	X	X
Arg^{136}	X	X	X	X
Tyr^{142}	X	X	X	X
Arg^{179}	X	X	Thr(5), X(2)	X
Tyr^{198}	X	X	X	X
Tyr^{199}	X	X	X	X

9–11 Å away from the putative iron-ligating tyrosines. However, a rearrangement in the Gln-11 side chain torsion angles coupled with a slight movement of the loop it resides on toward the binding cleft place the Gln-11 amide group in range to participate in iron ligation. Gln side chains are intrinsically flexible, and the average thermal factors for the atoms in the loop are considerably larger than the average B-factors for the protein, indicating that in the absence of bound iron, the loop is also flexible. It is probable that Gln-11 and the loop containing it become more ordered upon iron binding. A structural overlay of the iron-loaded HiFbpA structure with the structure of PhFbpA highlights the different strategies utilized by the two proteins to ligate iron (Fig. 3). Although Gln-11, Tyr-198, and Tyr-199 in PhFbpA appear to have similar iron-ligating counterparts (His-9, Tyr-195, and Tyr-196) in the HiFbpA structure, the two proteins differ dramatically the way that these and the additional (putative) groups surround the ligated iron. The phosphate anion in the HiFbpA structure appears to have been functionally replaced by Try-142 in PhFbpA (Fig. 3), and Glu-57 in the HiFbpA structure is replaced by an anion in PhfbpA positioned near formate 1. An additional anion bound at the position of formate 2 would complete the octahedral coordination sphere around the iron atom in PhFbpA.

The anions bind in basic pockets (Fig. 2) where they utilize polar interactions to interact with side chains from pairs of arginine residues. One of the oxygen atoms of formate 1 interacts simultaneously with terminal amino groups from Arg-10 and Arg-101, neutralizing electrostatic repulsions between the two Arg residues while the other oxygen atom from the formate interacts with the Nδ amine of Arg-10. Formate 2 binds at the N-terminal base of an α-helix comprising residues Arg-179/Glu-187 where it interacts through longer hydrogen bonds with Arg-136 and Arg-179 and shorter hydrogen bonds with main chain amide groups from Asp-178 and Arg-179. The two anions are separated by ~7 Å. Formate 1 appears to stabilize a closed conformation between the N- and C-terminal domains by participating in a hydrogen-bonding network among Arg-10, Arg-101, Tyr-142, and Tyr-198.

DISCUSSION

Inspection of the PhFbpA crystal structure reveals that it adopts the typical periplasmic ligand-binding protein (PLBP) fold that has been observed in almost all of the structurally characterized PLBPs to date. Even though most PLBPs from ABC transport systems share very little sequence homology and recognize a relatively large variety of ligands, almost all of these proteins possess bilobate structures in which the two domains are connected by a number of flexible β-strands located at the bottom of the ligand-binding cleft (33, 34). Despite the structural similarities to other PLBPs, FbpAs appear to be the only periplasmic transport proteins that are able to bind a free iron atom and transport it across the periplasmic space.

Although no metal ion is present in the PhFbpA crystal structure, an examination of binding pocket residue composition, structure, and sequence conservation data have allowed us to assign putative iron and anion-ligating residues with a high degree of confidence. A BLAST search (32) of the NCBI protein sequence data base has exposed 21 bacterial PhFbpA homologues with 41–80% sequence identity to PhFbpA (Table II). Of the putative iron-ligating residues we have assigned, Tyr-142, Tyr-198, and Tyr-199 are completely conserved in all of the homologues. Gln-11 is conserved in the majority of the homologues and is replaced by Glu or His in sequences where it differs with the exception in this case of the single lowest

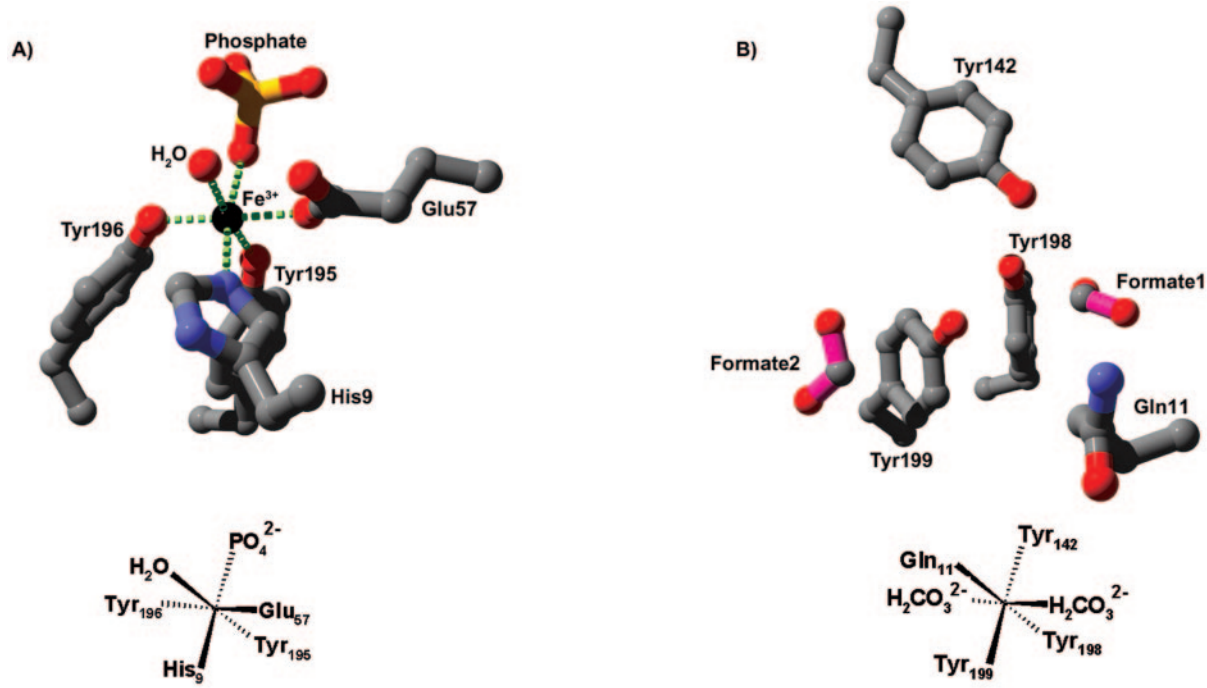

FIG. 3. **Comparison of observed Fe^{3+} coordination in HiFbpA (PDB code 1MRP) (*A*) and proposed Fe^{3+} coordination in PhFbpA (*B*).** The *top panels* show detailed views of the iron-binding pockets, and the *bottom panels* show schematic depictions of iron coordination. The two HiFbpA and PhFbpA structures were overlaid so that the binding pockets are viewed in the same orientation with respect to the overall protein structures. The binding cleft on each protein runs along the long axis of the page. In a side-by-side comparison, the binding sites present a completely different constellation of iron-coordinating ligands to the Fe^{3+} ion. The only feature shared between the two proteins is the utilization of a tyrosine ligand (Try-198 and Tyr-195 in PhFbpA and HiFbpA, respectively) in iron coordination at the bottom of the pocket. In PhFbpA, Gln-11 replaces the water ligand in HiFbpA, carbonate anions replace Tyr-196 and Glu-57, Tyr-199 replaces His-9, and Tyr142 replaces the phosphate.

homology sequence. The utilization of a Gln residue in iron coordination has been observed in the human transferrin N-lobe (29), whereas Glu and His residues have been observed coordinating iron in HiFbpA (28). The Gln-11, which resides on the protein surface and is completely solvated in the apo-structure probably contributes the least to the free energy of Fe^{3+} ion binding and could readily be replaced by a water molecule. Although literature describing biophysical characterizations of PhFbpA is sparse, the limited information available supports our claims. The iron-loaded protein possesses a peak visible absorbance (λ_{max}) at 419 nm, which is dramatically blue-shifted when compared with the same parameter from HiFbpA and Tf (λ_{max} of ~480 nM) (15). Because the relative effects of anions on the absorbance maximum are more subtle (−10 to −15 nM) (35), the large change in the absorbance maximum in PhFbpA can probably be ascribed to the fact that PhFbpA uses three tyrosine residues to coordinate iron *versus* the two utilized in all of the other structurally characterized FbpAs as well as in Tf and lactoferrin.

In addition to aiding in the assignment of iron-coordinating protein residues, the high resolution electron density maps have allowed for the unambiguous placement of the formate anions at two discrete binding sites on opposite sides of the binding pocket. Sequence comparison data (Table II) indicate that the residues utilized by PhFbpA to coordinate anions are almost completely conserved across all of the 21 homologous bacterial proteins, underscoring their functional significance. The formate anions bind in discrete conformations, utilizing hydrogen-bonding interactions among their oxygen atoms, arginyl amino groups, and main chain amide nitrogens (Fig. 2).

Formate 2 also takes advantage of a helix dipole as it binds at the N-terminal base of an α-helix, a phenomenon that is also observed for the phosphate anion in HiFbpA (28). Formate 1 also appears to play a key role in stabilizing a closed conformation of the binding pocket by stabilizing a hydrogen-bonding network among itself, Arg-10, and Arg-101 of the N-domain and linker region and tyrosines 142 and 198 of the C-terminal domain. Both anions are solvent-exposed, which may have implications in the iron loading and removal process in PhFbpA. Because formate was present at high (0.2 M) concentrations in the crystallization liquor and formate anions are smaller homologues of physiologically relevant carbonate anions, it is not surprising that we observe them bound to PhFbpA. It is probable that formate, while stabilizing domain closure, lacks the ability to simultaneously coordinate iron (see below), which has resulted in our observation of a closed apo-structure. As a corollary to the above statements, we can speculate that carbonate may serve as the physiological anion of choice in PhFbpA given the high degree of structural and electronic complementarity between the PhFbpA-binding pocket and the formate anions. Because the Fe^{3+} ion in PhFbpA is originally stripped from the host transferrin or lactoferrin, it is not unreasonable to conclude that these anion-binding sites would be filled by carbonate anions when present in ruminants given that the iron-loaded structures of transferrin and lactoferrin contain carbonate as the synergistic anion (36–40). The most plausible binding modes for the larger carbonate ions would be very similar to what we observe for formate (Fig. 3). Two oxygen atoms would be directed toward the binding pocket walls (exactly as we observed for the formates), whereas the third oxygen atoms from the respective carbonate atoms would extend outwards to coordinate iron from opposite sides. We conclude that the synergistic anions play dual roles in PhFbpA, induction of domain closure and Fe^{3+} ion ligation. By inducing domain closure, anions position key residues for iron ligation while still allowing for diffusion of materials to and from the binding site. If a sequential mechanism of iron binding and removal is utilized, anion binding may occur first to "prepare" the binding site for subsequent iron binding or conversely stripping of the anions from the binding

site may catalyze iron removal. The loop containing Gln-11, which is directed away from the binding site in this structure, could act as a "trapdoor" loop and gate iron loading/unloading. It is important to note that on the basis of our structural results, we cannot rule out phosphate as a physiological anion in PhFbpA because it is relatively small and would presumably bind in a similar fashion to formate/carbonate. Larger anions such as citrate may be tolerated but would have to direct a significant proportion of their mass out of the binding pocket because of steric constraints.

In summary, we have determined the first crystal structure of a new class of bacterial iron-binding proteins. We posit a model for octahedral iron coordination that utilizes three tyrosine residues, a glutamine and two carbonate anions. We continue to work toward obtaining an iron-loaded structure to confirm our hypotheses. We have also discovered 21 bacterial homologues that probably possess similar folds, coordinate iron utilizing a similar constellation of ligands, and play similar biological roles to PhFbpA in their respective organisms. Because iron is an essential nutrient, the structures of proteins in this class may aid in the design of antibacterial agents with therapeutic value.

Acknowledgments—ALS is supported by the Director, Office of Science, Office of Basic Energy Sciences, Materials Sciences Division of the U. S. Department of Energy under contract number DE-AC03-76SF00098 at Lawrence Berkeley National Laboratory. We also thank the staff at ALS for their excellent support.

REFERENCES

1. Whiteley, L. O., Maheswaran, S. K., Weiss, D. J., Ames, T. R., and Kannan, M. S. (1992) *J. Vet. Intern. Med.* **6,** 11–22
2. Ames, T. R., Markham, R. J., Opuda-Asibo, J., Leininger, J. R., and Maheswaran, S. K. (1985) *Can. J. Comp. Med.* **49,** 395–400
3. Marchart, J., Rehagen, M., Dropmann, G., Szostak, M. P., Alldinger, S., Lechleitner, S., Schlapp, T., Resch, S., and Lubitz, W. (2003) *Vaccine* **21,** 1415–1422
4. Conlon, J. A., Shewen, P. E., and Lo, R. Y. C. (1991) *Infect. Immun.* **59,** 587–591
5. Gilmour, N. J. L., Martin, W. B., Sharp, J. M., Thompson, D. A., Wells, P. W., and Donachie, W. (1983) *Res. Vet. Sci.* **35,** 80–86
6. Crosa, J. H. (1984) *Annu. Rev. Microbiol.* **38,** 69–89
7. Weinberg, E. D. (1984) *Physiol. Rev.* **64,** 65–102
8. Schryvers, A. B., and Stojiljkovic, I. (1999) *Mol. Microbiol.* **32,** 1117–1123
9. Wessling-Resnick, M. (1999) *Crit. Rev. Biochem. Mol. Biol.* **34,** 285–314
10. Mietzner, T. A., and Morse, S. A. (1994) *Annu. Rev. Nutr.* **14,** 471–493
11. Gray-Owen, S. D., and Schryvers, A. B. (1996) *Trends Microbiol.* **4,** 185–191
12. Jarosik, G. P., Maciver, I., and Hansen, E. J. (1995) *Infect. Immun.* **63,** 710–713
13. Chen, C.-Y., Berish, S. A., Morse, S. A., and Mietzner, T. A. (1993) *Mol. Microbiol.* **10,** 311–318
14. Kirby, S. D., Gray-Owen, S. D., and Schryvers, A. B. (1997) *Mol. Microbiol.* **25,** 979–987
15. Kirby, S. D., Lainson, F. A., Donachie, W., Okabe, A., Tokuda, M., Hatase, O., and Schryvers, A. B. (1998) *Microbiology* **144,** 3425–3436
16. Tam, R., and Saier, M. H. (1993) *Microbiol. Rev.* **57,** 320–346
17. Adhikari, P., Kirby, S. D., Nowalk, A. J., Veraldi, K. L., Schryvers, A. B., and Mietzner, T. A. (1995) *J. Biol. Chem.* **42,** 25142–25149
18. Shouldice, S. R., Dougan, D. R., Skene, R. J., Tari, L. W., McRee, D. E., Yu, R.-H., and Schryvers, A. B. (2003) *J. Biol. Chem.* **278,** 11513–11519
19. Otwinowski, Z., and Minor, W. (1997) *Methods Enzymol.* **267,** 307–326
20. Weeks, C. M., and Miller, R. (1999) *J. Appl. Crystallogr.* **32,** 120–124
21. De La Fortelle, E., and Bricogne, G. (1997) *Methods Enzymol.* **276,** 472–494
22. McRee, D. E. (1999) *J. Struct. Biol.* **125,** 156–165
23. Brunger, A. T., Adams, P. D., Clore, G. M., DeLano, W. L., Gros, P., Grosse-Kunstleve, R. W., Jiang, J. S., Kuszewski, J., Nilges, M., Pannu, N. S., Read, R. J., Rice, L. M., Simonson, T., and Warren, G. L. (1998) *Acta Crystallogr. Sec. D* **54,** 905–921
24. Collaborative Computational Project Number 4. (1994) *Acta Crystallogr. Sec. D* **50,** 760–763
25. Morris, R. J., Perrakis, A., and Lamzin V. S. (2002) *Acta Crystallogr. Sec. D* **58,** 968–975
26. Murshudov, G. N., Vagin, A. A., and Dodson, E. J. (1997) *Acta Crystallogr. Sec. D* **53,** 240–255
27. Holm, L., and Sander, C. (1997) *Nucleic Acids Res.* **25,** 231–234
28. Bruns, C. M., Norwalk, A. J., Avrai, A. S., McTigue, M. A., Vaughan, K. A., Mietzner, T. A., and McRee, D. E. (1997) *Nat. Struct. Biol.* **4,** 919–924
29. Yang, A. H., MacGillivray, R. T., Chen, J., Luo, Y., Wang, Y., Brayer, G. D., Mason, A. B., Woodworth, R. C., and Murphy, M. E. (2000) *Protein Sci.* **9,** 49–52
30. Peterson, N. A., Arcus, V. L., Anderson, B. F., Tweedie, J. W. Jameson, G. B., and Baker, E. N. (2002) *Biochemistry* **41,** 14167–14175
31. Mizutani, K., Mikami, B., and Hirose, M. (2001) *J. Mol. Biol.* **309,** 937–947
32. Brown, M. P. S., Grundy, W. N., Lin, D., Cristiani, N., Sugnet, C. M., Ares, J., and Haussler, D. (1999) *Nucleic Acids Res.* **25,** 3389–3402
33. Quiocho, F. A. (1990) *Philos. Trans. R. Soc. Lond-Biol. Sci.* **326,** 341–351
34. Quiocho, F. A., and Ledvina, P. S. (1996) *Mol. Microbiol.* **20,** 17–25
35. Dhungana, S., Taboy, C. H., Anderson, D. S., Vaughan, K. G., Aisen, P., Meitzner. T. A., and Crumbliss, A. L. (2003) *Proc. Natl. Acad. Sci. U. S. A.* **100,** 3659–3664
36. MacGillivray, R. T. A., Moore, S. A., Chen, J., Anderson, B. F., Baker, H., Luo, Y. G., Bewley, M., Smith, C. A., Murphy, M. E. P., Wang, Y., Mason, A. B., Woodworth, R. C., Brayer, G. D., and Baker, E. N. (1998) *Biochemistry* **37,** 7919–7928
37. Baker, H. M., Mason, A. B., He, Q. Y., MacGillivray, R. T., and Baker, E. N. (2001) *Biochemistry* **40,** 11670–11675
38. Hall, D. R., Hadden, J. M., Leonard, G. A., Bailey, S., Neu, M., Winn, M., and Lindley, P. F. (2002) *Acta Crystallogr. D. Biol. Crystallogr.* **58,** 70–80
39. Kurokawa, H., Mikami, B., and Hirose, M. (1995) *J. Mol. Biol.* **254,** 196–207
40. Moore, S. A., Anderson, B. F., Groom, C. R., Haridas, M., and Baker, E. N. (1997) *J. Mol. Biol.* **274,** 222–236

Crystal Structure of *Pasteurella haemolytica* Ferric Ion-binding Protein A Reveals a Novel Class of Bacterial Iron-binding Proteins

Stephen R. Shouldice, Douglas R. Dougan, Pamela A. Williams, Robert J. Skene, Gyorgy Snell, Daniel Scheibe, Shane Kirby, David J. Hosfield, Duncan E. McRee, Anthony B. Schryvers and Leslie W. Tari

J. Biol. Chem. 2003, 278:41093-41098.
doi: 10.1074/jbc.M306821200 originally published online July 25, 2003
